Selective expression of mutant huntingtin during development recapitulates characteristic features of Huntington's disease

Aldrin E. Molero[a,b,c,d,1], Eduardo E. Arteaga-Bracho[a,b,d,e,1], Christopher H. Chen[e], Maria Gulinello[d,e], Michael L. Winchester[a,b,c,d], Nandini Pichamoorthy[a,b,c,d], Solen Gokhan[a,b,c,d], Kamran Khodakhah[c,e,f], and Mark F. Mehler[a,b,c,d,e,f,g,h,i,j,2]

[a]Roslyn and Leslie Goldstein Laboratory for Stem Cell Biology and Regenerative Medicine, Albert Einstein College of Medicine, Bronx, NY 10461; [b]Institute for Brain Disorders and Neural Regeneration, Albert Einstein College of Medicine, Bronx, NY 10461; [c]The Saul R. Korey Department of Neurology, Albert Einstein College of Medicine, Bronx, NY 10461; [d]Rose F. Kennedy Center for Research on Intellectual and Developmental Disabilities, Albert Einstein College of Medicine, Bronx, NY 10461; [e]Dominick P. Purpura Department of Neuroscience, Albert Einstein College of Medicine, Bronx, NY 10461; [f]Department of Psychiatry and Behavioral Sciences, Albert Einstein College of Medicine, Bronx, NY 10461; [g]Einstein Cancer Center, Albert Einstein College of Medicine, Bronx, NY 10461; [h]Ruth L. and David S. Gottesman Institute for Stem Cell Biology and Regenerative Medicine, Albert Einstein College of Medicine, Bronx, NY 10461; [i]Center for Epigenomics, Albert Einstein College of Medicine, Bronx, NY 10461; and [j]Institute for Aging Research, Albert Einstein College of Medicine, Bronx, NY 10461

Edited by David E. Housman, Massachusetts Institute of Technology, Cambridge, MA, and approved April 5, 2016 (received for review March 8, 2016)

Recent studies have identified impairments in neural induction and in striatal and cortical neurogenesis in Huntington's disease (HD) knock-in mouse models and associated embryonic stem cell lines. However, the potential role of these developmental alterations for HD pathogenesis and progression is currently unknown. To address this issue, we used BACHD:CAG-Cre^{ERT2} mice, which carry mutant *huntingtin* (m*Htt*) modified to harbor a floxed exon 1 containing the pathogenic polyglutamine expansion (Q97). Upon tamoxifen administration at postnatal day 21, the floxed m*Htt*-exon1 was removed and m*Htt* expression was terminated (Q97^{CRE}). These conditional mice displayed similar profiles of impairments to those mice expressing m*Htt* throughout life: (*i*) striatal neurodegeneration, (*ii*) early vulnerability to NMDA-mediated excitotoxicity, (*iii*) impairments in motor coordination, (*iv*) temporally distinct abnormalities in striatal electrophysiological activity, and (*v*) altered corticostriatal functional connectivity and plasticity. These findings strongly suggest that developmental aberrations may play important roles in HD pathogenesis and progression.

neurodegeneration | prodromal | plasticity

Huntington's disease (HD) is an inherited neurodegenerative disorder caused by abnormal expansion of a polyglutamine tract in the amino terminal end of the protein, huntingtin (Htt). HD is characterized by the onset and progression of motor alterations frequently commencing during the fourth decade of life and associated with degeneration of the striatum, cortex, and other brain areas. Research initiatives in the field have traditionally focused on defining the biological processes mediating neuronal dysfunction and death during adult life. More recently, our studies and others have shown that the HD pathogenic mutation impairs the specification and maturation of striatal medium spiny neurons (MSNs), the primary target of HD neurodegeneration, and alters cortical progenitor cell divisions and neurogenesis by causing deregulation of mitotic spindle orientation (1, 2). Although the role of these diverse developmental defects for HD pathogenesis remains undefined, they have the potential to impair the integrity of striatal and cortical neuronal homeostasis and function through multiple inductive interactions. Indeed, these changes may provide an explanation for studies, including the Neurobiological Predictors of Huntington's Disease (PREDICT-HD) and TRACK-HD studies, showing electrophysiological abnormalities, discrete brain structural as well as volumetric changes, and cognitive and motor deficits occurring long before disease onset (3–8). We therefore propose that selective exposure to mutant *Htt* (m*Htt*) during neural development can recapitulate characteristic features of HD. To examine this possibility, we used a conditional m*Htt*-ablation model allowing selective developmental expression of m*Htt*.

Results

The Generation of BACHD Mice Selectively Expressing m*Htt* During Development. We interbred BACHD mice (9) carrying the full-length human m*Htt* gene modified to harbor a floxed exon 1 coding for 97 polyglutamine repeats (HD juvenile repeat range) with mice carrying the tamoxifen-inducible Cre recombinase (CRE) driver system (CAG-Cre/Esr1) (10). Their offspring were subsequently treated with tamoxifen at postnatal day (PND) 21 to generate mice expressing m*Htt*: (*i*) only during development (Q97^{CRE}), (*ii*) during development and adult life (Q97), and (*iii*) in WT controls not expressing m*Htt* (WT). In 3-mo-old mice, the efficiency of m*Htt* tamoxifen-induced brain gene ablation was examined at genomic (Fig. S1 *A* and *B*), transcript, and protein levels (Fig. 1 and Fig. S1 *C* and *D*). Quantitative real-time PCR (QRT-PCR) analysis using primers targeting the floxed region of m*Htt* revealed a 98.2% reduction of the genomic amplicon in

Significance

Research initiatives in Huntington's disease (HD) have traditionally focused on defining the biological processes mediating neuronal dysfunction and death during adult life. In contrast to these classical approaches, we have shown that selective exposure to the pathogenic protein during development recapitulates characteristic features of HD. These findings support the hypothesis that putative HD-associated developmental impairments in neurogenesis contribute to regional cellular vulnerabilities to late-life stressors leading to dysfunction culminating in cell death. An implication of our findings is that the spectrum of developmental alterations can be held in check for many decades after the birth of these vulnerable neuronal subtypes, thus defining a previously unidentified window for therapeutic interventions at a time when irreversible neural degeneration has not yet occurred.

Author contributions: A.E.M., E.E.A.-B., K.K., and M.F.M. designed research; A.E.M., E.E.A.-B., C.H.C., M.G., M.L.W., N.P., and S.G. performed research; A.E.M., E.E.A.-B., C.H.C., M.G., K.K., and M.F.M. analyzed data; and A.E.M., E.E.A.-B., S.G., K.K., and M.F.M. wrote the paper.

The authors declare no conflict of interest.

This article is a PNAS Direct Submission.

[1]A.E.M. and E.E.A.-B. contributed equally to this work.

[2]To whom correspondence should be addressed. Email: mark.mehler@einstein.yu.edu.

This article contains supporting information online at www.pnas.org/lookup/suppl/doi:10.1073/pnas.1603871113/-/DCSupplemental.

www.pnas.org/cgi/doi/10.1073/pnas.1603871113

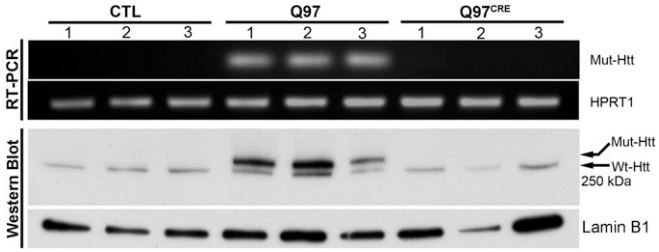

Fig. 1. CRE^{ER} yields highly efficient levels of mHtt excisional recombination in Q97^{CRE} mice. In contrast to striatal Q97 specimens, RT-PCR amplicons using primers that selectively detect the presence of mutant exon 1 of the Htt cDNA (*Top*) and Western blot analysis probed with the mAb 2166 anti-Htt antibody (~350 kDa, *Bottom*) show no discernible bands in control and Q97^{CRE} striatal specimens ($n_{per\ strain}$ = 3).

Q97^{CRE} compared with Q97 mice (Fig. S1 *A* and *B*). Further analysis of m*Htt* RNA expression showed a 99.8% reduction of transcript expression in Q97^{CRE} compared with WT mice (Fig. 1, *Upper* and and Fig. S1 *C* and *D*). Accordingly, no m*Htt* protein was detected by Western blot analysis (Fig. 1, *Lower*). Consistent with previous studies (10), we also verified efficient levels of recombination throughout the neuraxis and in nonneural tissues (Fig. S2). These observations validate the use of the BACHD mouse model to study the selective effects of m*Htt* expression during development.

Q97^{CRE} Mice Display HD-Like Profiles of Striatal Vulnerability to Cell Death. Striatal vulnerability to neurodegeneration is a seminal hallmark of HD. To investigate the presence of HD striatal pathology in Q97^{CRE} mice, we studied gross morphological changes in brain specimens of 9-mo-old mice. We found that striatal volumes [$F_{(2,12)}$ = 1.28, P = 0.311], as well as the numbers of striatal NeuN^{+} neuronal species [$F_{(2,21)}$ = 1.86, P = 0.18], were not different between the three experimental groups. To identify neurodegenerative changes more thoroughly, we used toluidine blue staining of semithin striatal sections from the lateral aspect of the striatum (Fig. 2 *A* and *B*), a region previously shown to display the largest number of degenerating neurons in Q97 mice (9). Degenerating cells in the striatum appear dark when stained with toluidine blue. We found that compared with WT specimens [1.1%, 0.6–1.9 coefficient interval (CI95%)], both Q97^{CRE} (6.6%, 5.3–8.1 CI95%) and Q97 (7.6%, 6.3–9.1 CI95%) specimens showed larger numbers of darkly stained degenerating neurons (Fig. 2*A*), many of which exhibited atrophic morphologies (Fig. 2*A*, arrowheads). Electron microscopic techniques further confirmed the presence of darkly stained atrophic neurons displaying morphological features of neurodegeneration, not only in the Q97 striatum but also in the Q97^{CRE} striatum (Fig. 2 *C–E*). The neuronal identity of degenerating cells was confirmed by the detection of axosomatic synapses in these species (Fig. 2 *C*, outlined box and *D*). These results suggest that selective exposure to mHtt during neural development creates a state of striatal cell vulnerable to cell death.

One provocative additional possibility is that this vulnerability might even be present early in life. In support of this possibility, previous studies have shown that early in life, HD mouse models exhibit an increased striatal vulnerability to NMDA-mediated excitotoxicity both in vivo and in vitro (11, 12). However, these studies do not clarify whether the cellular vulnerability is a consequence of developmental abnormalities or the continuing effects of the mutant protein during adult life. To investigate this seminal issue, we injected either the NMDA agonist quinolinic acid (QA) or PBS unilaterally into the corresponding dorsal aspect of the striatum of 3-mo-old Q97^{CRE} mice. Seven days postinjection, striatal lesions were quantified using Fluoro-Jade C (Millipore), a cell death marker. PBS-mediated lesions were similar across all experimental groups [$F_{(2,11)}$ = 0.245, P = 0.786], and were smaller than those lesions resulting from QA [$t_{(8)}$ = 4.5, $t_{(6)}$ = 8.2, and $t_{(8)}$ = 4.6; P < 0.01 for Q97^{CRE}, Q97, and control (CTL) mice, respectively]. Moreover, both Q97^{CRE} and Q97 striata displayed approximately twofold larger QA lesions compared with those lesions seen in WT specimens [$F_{(2,11)}$ = 10.64, P = 0.002; Tukey's honest significant difference (HSD) post hoc test, P = 0.031 and P = 0.002, respectively; Fig. 2 *F–I*, asterisks]. These results reveal

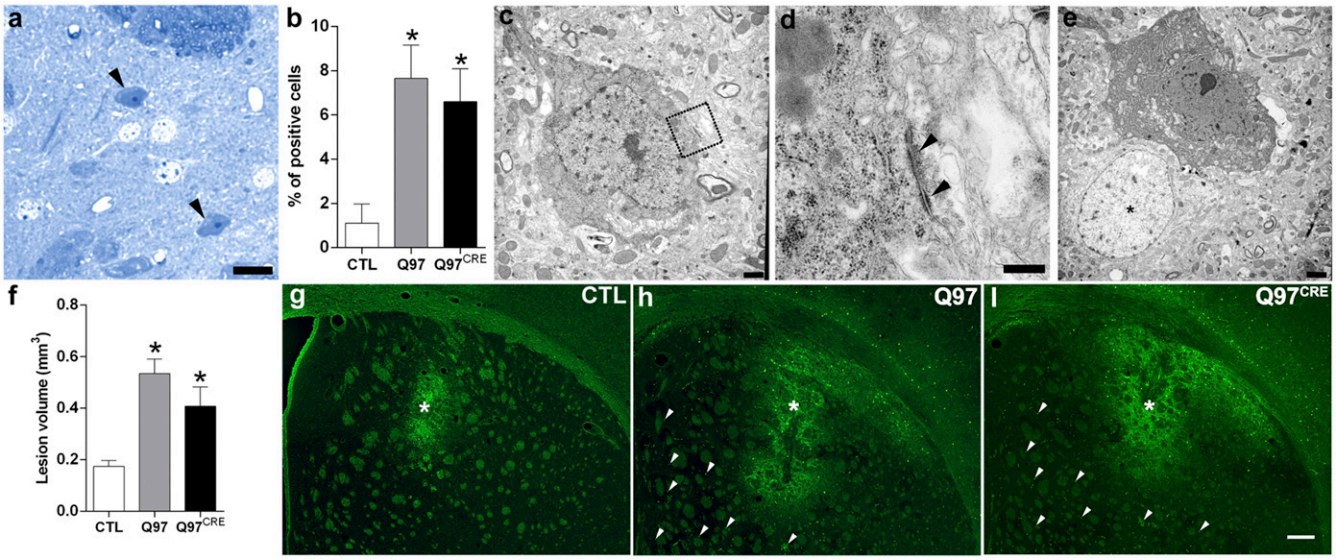

Fig. 2. Q97^{CRE} mice display late-life appearance of striatal cellular degeneration and enhanced vulnerability to QA. Semithin sections (1 μm) of 9-mo-old striatum of female mice show that the number of darkly stained degenerating toluidine blue-positive cells was significantly higher in both Q97^{CRE} (*A*, arrowheads) and Q97 mice compared with CTL mice (*B*, percentage ± 95% confidence interval). (*C–E*) Electron micrographic images showing representative degenerating cells in the striatum of Q97^{CRE} mouse specimens. *D* corresponds to the boxed area in *C*, illustrating the presence of an axosomatic synapse (arrowheads). The asterisk in *E* identifies the nucleus of a normal striatal cell. (*G–I*) Representative striatal specimens that received a single intrastriatal injection of QA and were thereafter treated with Fluoro-Jade C to label dying cells (an asterisk depicts the site of the QA lesion). Arrowheads in *H* and *I* depict scattered Fluoro-Jade C–positive cells throughout the striatum. (Scale bars: *A*, 100 μm; *D*, 0.33 μm; *C* and *E*, 1 μm; *I*, 220 μm.) *P < 0.05 for statistical comparisons between CTL and either Q97^{CRE} or Q97 specimens.

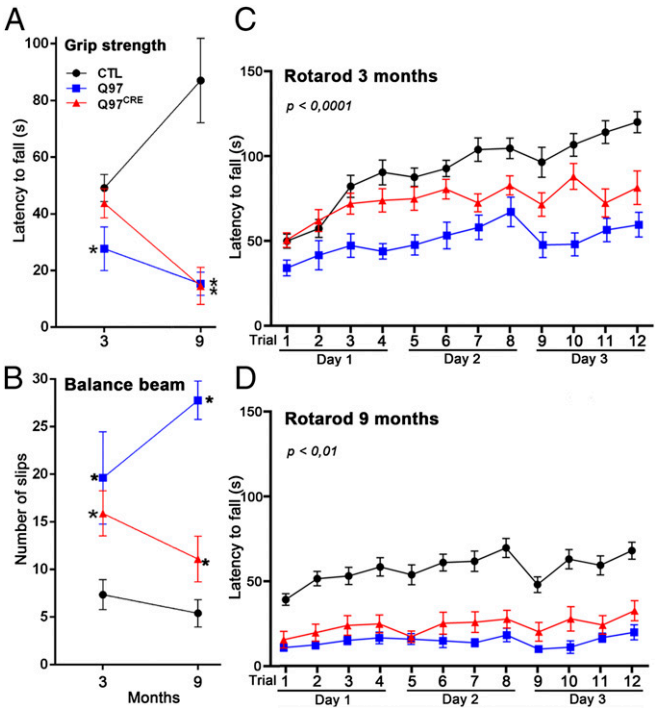

Fig. 3. Q97^{CRE} mice have analogous, although less severe, motor deficits compared with Q97 mice. Behavioral examinations were performed at 3 and 9 mo of age in a single cohort of female mice from each experimental group (n = 10, n = 9, and n = 12 for Q97^{CRE}, Q97, and CTL mice, respectively). Compared with CTL mice, both Q97^{CRE} and Q97 mice displayed deficits in limb grip strength (paw grip endurance hanging wire test) at 9 mo of age (*A*) and a higher number of slips in the balance beam test at 3 and 9 mo of age (*B*). (*C* and *D*) Consistently, repeated rotarod tests at 3 and 9 mo of age also revealed significant deficits in motor coordination in Q97^{CRE} mice. Individual values represent the mean ± SEM. *P* values (*) depicted at the top or next to each experimental group in *A* and *B* represent the statistical comparison with corresponding age-matched controls.

that mHtt displays an active role in sculpting this cellular vulnerability to neurodegeneration during neural development.

Q97^{CRE} Mice Partially Recapitulate Motor Deficits of Q97 Mice. Progressive motor alterations are a clinical hallmark of HD, and they appear years before pathological changes are observed in patients with HD. However, whether selective developmental expression of mHtt is sufficient to produce progressive behavioral impairments remains unknown. We performed comparative behavioral analysis in a cohort of Q97^{CRE}, Q97, and CTL mice at 3 and 9 mo of age (Fig. 3). To control for the confounding effects of weight in our behavioral examinations, all analyses were adjusted for this variable (13). We studied muscle strength with the Grip test. At 3 mo of age, Q97 but not Q97^{CRE} mice displayed shorter latencies to fall in comparison to CTL mice [$F_{(2,27)}$ = 2.86, P = 0.073; Tukey's HSD post hoc test, P = 0.045; Fig. 3*A*]. However, at 9 mo of age, both Q97 and Q97^{CRE} mice exhibited shorter latencies to fall compared with CTL mice [$F_{(2,27)}$ = 20.68, P < 0.0001; Fig. 3*A*]. These observations indicate the presence of progressive reductions in muscle strength for both Q97^{CRE} and Q97 mice. To examine motor coordination, we measured the number of slips of the mice using the balance beam test. Compared with CTL mice, both 3- and 9-mo-old Q97^{CRE} and Q97 mice displayed higher numbers of slips [$F_{(2,26)}$ = 3.92, P = 0.032 and $F_{(2,28)}$ = 39.4, P < 0.0001, respectively; Fig. 3*C*]. In addition, the number of slips at 9 mo, but not at 3 mo, were significantly higher in Q97^{CRE} compared with Q97 mice [$t_{(16)}$ = 4.99, P = 0.0001 and $t_{(15)}$ = 0.59, P = 0.6, respectively]. To examine motor coordination further, we used the rotarod test (Rotamex-5; Columbus Instruments). We assessed differences among groups using a mixed linear ANOVA model with repeated measurements. This model revealed differences in the latencies of mice at 3 mo (Fig. 3*B*) and 9 mo (Fig. 3*D*) of age to fall across all experimental models examined. Compared with CTL mice, the individual latencies to fall of Q97^{CRE} and Q97 mice were shorter at both 3 mo [$F_{(1,22)}$ = 8.40, P = 0.0122 and $F_{(1,21)}$ = 34.4, P < 0.01 for genotype effects, respectively; Fig. 3*B*] and 9 mo [$F_{(1,24)}$ = 5.75, P = 0.02 and $F_{(1,23)}$ = 8.98, P < 0.01 for genotype effects, respectively; Fig. 3*D*] of age. Moreover, although comparisons between mutant strains (Q97^{CRE} and Q97) revealed that Q97^{CRE} mice displayed longer latencies to fall than Q97 mice at 3 mo of age [$F_{(1,17)}$ = 7.73, P = 0.013 for genotype effect; Fig. 3*B*], but not at 9 mo of age [$F_{(1,17)}$ = 0.08, P = 0.77 for genotype effect; Fig. 3*D*], indicating the preferential influences of mHtt during early but not later life. Overall, these data demonstrate that Q97^{CRE} mice display deficits in motor coordination, suggesting that selective expression of mHtt during the developmental period partially recapitulates the motor deficits of HD.

Q97^{CRE} and Q97 Mice Display Age-Dependent Alterations in Striatal Spiking Activity. A number of studies have demonstrated defects in in vivo striatal spiking activity (14, 15) and in vitro age-dependent alterations in different striatal cell types (14, 16, 17) in various HD mouse models. We sought to determine whether mHtt-associated developmental effects contribute to these electrophysiological alterations. We implanted a drivable microarray to record single-unit activities within the dorsolateral striatum of behaving 3- to 4-mo-old and 9- to 12-mo-old Q97^{CRE} mice (Fig. 4). The recorded units were classified according to their waveform (18) as either putative MSNs (Fig. 4*A*) or GABAergic interneurons (GINs; Fig. 4*B*). The proportions of units classified as MSNs and GINs were not different between the three genotypes in 3- to 4-mo-old and 9- to 12-mo-old mice [~50% for MSN and GINs at both age ranges; $\chi^2_{(2)}$ = 0.566, P = 0.753 and $\chi^2_{(2)}$ = 1.877, P = 0.391, respectively]. At 3 to 4 mo of age, the firing rate of MSNs was similar among the experimental groups [$H_{(2,66)}$ = 0.557, P = 0.756; Fig. 4*C*), although the coefficient of variation (CV) of the interspike interval (ISI) of MSNs was increased in both Q97^{CRE} and Q97 mice [$F_{(2,66)}$ = 8.22, P < 0.001, P = 0.032; Fig. 4*D*]. In contrast, the firing rate of striatal GINs was decreased [$H_{(2,60)}$ = 16.31, P < 0.001; Fig. 4*E*] in both Q97^{CRE} and Q97 mice. Because the firing rate of GINs was different among groups, we used the SD of the ISI as a more appropriate measure of spiking variability than the CV of the ISI. We observed that the SD of the ISI for GINs was increased for both Q97 and Q97^{CRE} mice [$F_{(2,60)}$ = 3.19, P = 0.048; Fig. 4*F*]. These observations during the 3- to 4-mo age range suggest generalized alterations in the striatal spiking activity as a result of the presence of mHtt during development. At 9 to 12 mo of age, the MSN firing rate was similar among all genotypes [$H_{(2,75)}$ = 1.50, P < 0.472; Fig. 4*G*]. However, the CV of the ISI of MSNs was decreased [$F_{(2,74)}$ = 7.09, P < 0.001; Fig. 4*H*]. For GINs, both the firing rate [$H_{(2,68)}$ = 0.56, P < 0.752; Fig. 4*I*] and the CV of the ISI [$F_{(2,68)}$ = 1.69, P < 0.192; Fig. 4*J*] were similar across all experimental groups. Therefore, by contrast, during the 9- to 12-mo age range, we observed that alterations in striatal spiking activity were selective for MSNs rather than GINs. These overall observations demonstrate that both MSNs and GINs display age-dependent alterations in their spiking activity. Moreover, our results reveal that mHtt-associated developmental defects contribute to alterations in both age- and neuronal subtype-dependent striatal spiking activity.

Q97^{CRE} and Q97 Mice Display Alterations in Corticostriatal Communications and Plasticity. Several electrophysiological alterations in the corticostriatal pathway have been implicated in HD. They include late-onset loss of cortical innervation of the striatum and defects in corticostriatal plasticity in acute brain slices from HD mouse models (19–21). However, whether selective expression of the mHtt during the developmental period contributes to corticostriatal dysfunction is not known. We addressed this issue by analyzing corticostriatal

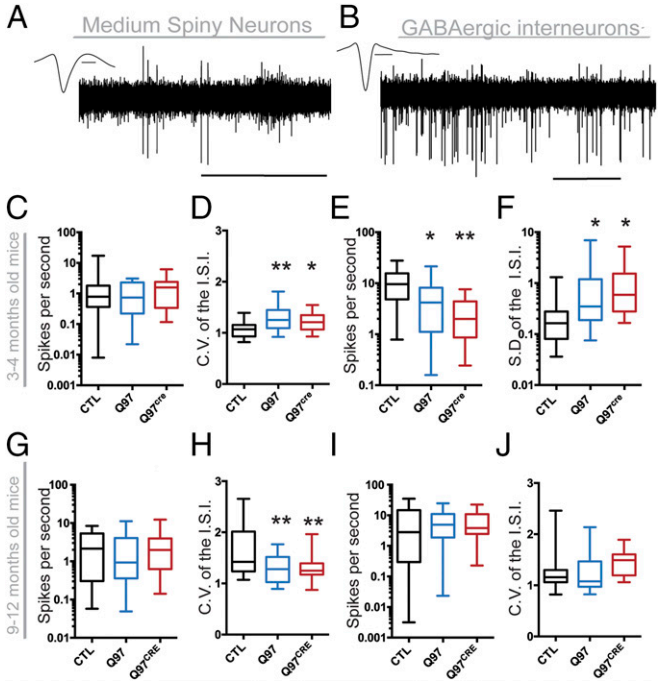

Fig. 4. Both Q97^{CRE} and Q97 mice exhibit abnormal striatal electrophysiological activity. (*A* and *B*) Drivable microarrays were implanted within the dorsolateral striatum to record the single-unit activity of awake, behaving 3- to 4-mo-old and 9- to 12-mo-old mice. (*C*) In 3- to 4-mo-old mice, MSN firing rates from Q97 ($n = 22$) and Q97^{CRE} ($n = 20$) mice were similar to CTL ($n = 27$) mice. (*D*) ISI CV was increased in Q97 and Q97^{CRE} MSNs compared with CTL MSNs. (*E*) GIN firing rates from Q97 ($n = 21$) and Q97^{CRE} ($n = 15$) mice were significantly lower than in CTL ($n = 27$) mice. (*F*) In comparison to CTL units, the SD of the ISI of GINs was higher for both Q97 and Q97^{CRE} units. In 9- to 12-mo-old mice, MSN firing rates from Q97 ($n = 23$) and Q97^{CRE} ($n = 27$) mice were similar to CTL ($n = 26$) mice (*G*); however, the CV of the ISI was decreased in both Q97 ($n = 23$) and Q97^{CRE} ($n = 27$) mice in comparison to CTL ($n = 26$) units (*H*). No differences were detected in the firing rate (*I*) or the CV of the ISI of GINs (*J*). Data are shown as whisker box plots representing the median (at the center), interquartile range (outer box), and minimum and maximum values (whiskers). *$P < 0.05$; **$P < 0.001$.

pathway properties in 9- to 12-mo-old freely moving Q97^{CRE} mice. We implanted an eight-wire microarray in the striatum and an electrical microstimulator within the motor cortex of experimental mice. We then assessed the effects of cortical stimulation on the responsivity of striatal unit activity. We found that cortical stimulation induced the following responses: (*i*) excitation, defined as the transient increase in the firing rate (Fig. S3*A*); (*ii*) inhibition, characterized by the transient suppression of striatal activity (Fig. S3*B*); and (*iii*) no response (Fig. S3*C*). Because the motor cortex provides the primary excitatory input to the dorsolateral striatum, we focused our analysis on units displaying excitation as a response. We found that there is an ~20% decrease of striatal units displaying excitatory response in both Q97 and Q97^{CRE} mice compared with CTL mice [$\chi^2_{(2)} = 15.53$, $P < 0.0003$; Fig. 5*A*]. These findings suggest a decrease in functional corticostriatal connectivity. However, we observed that in those cells displaying excitation, the number of spikes elicited after cortical stimulation [$H_{(2,70)} = 3.923$, $P = 0.140$; Fig. 5*B*] and the excitatory response latency [$H_{(2,70)} = 2.422$, $P = 0.297$; Fig. 5*C*] were similar among all genotypes. This finding suggests that the remaining cortical inputs retain the ability to modulate the firing of striatal neurons in the HD mouse models. Our overall observations imply that the reduction of the cortical input to striatal cells is a consequence of selective developmental expression of mHtt.

It is known that decreased inputs to the striatum are able to alter corticostriatal plasticity (22, 23). Therefore, we hypothesized that the relative corticostriatal functional disconnection is also able to impair corticostriatal plasticity in HD. In a previous work, we have shown that delivery of high-frequency stimulation (HFS) to the motor cortex of freely moving mice is able to induce bidirectional striatal plasticity (24). Using the same experimental paradigm, we observed striatal units that displayed decreased [long-term depression (LTD); Fig. S3*D*] or increased [long-term potentiation (LTP); Fig. S3*E*] evoked spikes post-HFS in comparison to pre-HFS in all experimental mice. We find that the proportion of units displaying LTP was increased ~25% at the expense of units displaying LTD in both Q97 and Q97^{CRE} mice in comparison to CTL mice [$\chi^2_{(2)} = 19.02$, $P < 0.0001$; Fig. 5*D*]. For units that we categorized as undergoing LTD, the ratio of extra spikes post-HFS/pre-HFS was comparable among all experimental mice [$H_{(2,45)} = 3.382$, $P = 0.184$; Fig. 5*E*]. Similarly, in both Q97 and Q97^{CRE} mouse units undergoing LTP display, there were no differences in the ratio of extra spikes post-HFS over pre-HFS

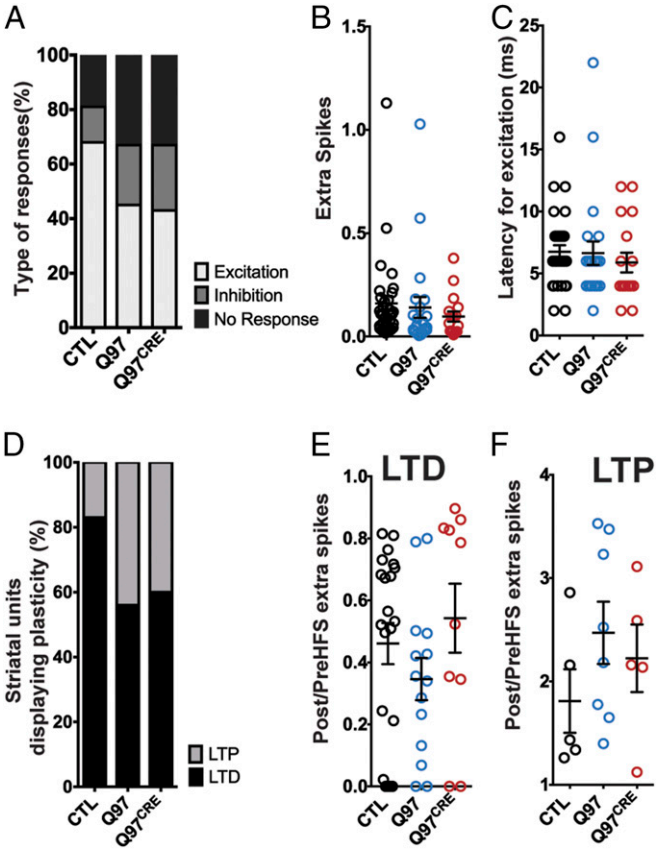

Fig. 5. Q97^{CRE} mice display impairments in corticostriatal connectivity and plasticity. (*A*) Proportion of cells exhibiting an excitatory response to cortical stimulation was reduced in both Q97 and Q97^{CRE} mice in comparison to CTL mice (CTL = 47, Q97 = 49, and Q97^{CRE} = 47 cells). (*B*) Correspondence to the summary data for the number of extra spikes elicited in striatal units displaying excitation by cortical stimulation (CTL = 32, Q97 = 22, and Q97^{CRE} = 17 cells). The number of extra spikes was similar among all experimental groups. (*C*) Correspondence to the summary data for latency to elicited excitation in striatal units by cortical stimulation. The latency was similar among all experimental groups. (*D*) Proportion of striatal cells undergoing LTP is increased in both Q97 and Q97^{CRE} mice in comparison to CTL mice (CTL = 27, Q97 = 22, and Q97^{CRE} = 15 cells). (*E* and *F*) Summary data for striatal units undergoing LTD or LTP, respectively, for all experimental groups. (*E*) Ratio of spikes before and after HFS for cells undergoing LTD was not statistically different among genotypes. (*F*) Ratio of spikes before and after HFS for cells undergoing LTP among all experimental groups was not statistically different among genotypes. We used six to eight mice per genotype in all of the experimental paradigms. The mean and SEM are displayed in *B*, *C*, *E*, and *F*, and each individual point represents a striatal unit.

compared with CTL mice [$H_{(2,18)} = 2.464$, $P = 0.304$; Fig. 5*F*]. These overall results suggest that the relative HD-mediated corticostriatal disconnection has the potential to alter bidirectional striatal plasticity and, additionally, that previously demonstrated mHtt-associated developmental alterations in both the striatum and cortex may furnish the regional substrates to mediate these dynamic processes.

Discussion

We have shown that selective exposure to mHtt during development recapitulates characteristic features of the HD phenotype. The findings in Q97^{CRE} mice of striatal degeneration, early susceptibility to NMDA-mediated excitotoxicity, progressive motor coordination deficits, impairments in striatal spiking activity, and defects in corticostriatal plasticity and functional connectivity suggest that developmental abnormalities play an important role in HD pathogenesis.

We have postulated that m*Htt*-associated developmental dysfunction contributes to HD neurodegeneration (1). We and other groups have previously shown impairments in early embryonic development and stem cell-mediated striatal neurogenesis in HD mouse and cellular models (1, 25–27). These impairments may exert long-term disease-modifying effects (27), including selective neuronal vulnerability to degeneration. This concept is supported by the fact that Q97^{CRE} mice display HD-like neurodegeneration.

Ablation of m*Htt* after PND21 in Q97^{CRE} mice resulted in reductions in muscle strength and alterations in locomotor activity and motor coordination. However, these defects were not as severe as those defects observed in Q97 mice. These partial defects in the Q97^{CRE} mice suggest that developmental mechanisms alone may not be sufficient to yield the entire spectrum of HD pathologies, thus potentially supporting a disease model encompassing two pathogenic components: one developmental and the other reflecting the ongoing toxic effects of m*Htt*. As a corollary, selective targeting of m*Htt* during postnatal life may not be sufficient to prevent or cause complete rescue of the HD phenotype. Consistently, although cumulative studies have reported that postnatal ablation or reduction of m*Htt* delays HD onset (28, 29), prolongs longevity of mice (28, 30, 31), stabilizes brain atrophy (28, 32), and improves motor functions (28, 33), targeting of the pathogenic protein does not lead to full reversal of the HD phenotype. It is also possible that these profiles of partial recovery reflected the fact that gene targeting was performed at a time when the deleterious effects of m*Htt* had already resulted in irreversible pathophysiological changes. However, Wang et al. (30) targeted m*Htt* well before the establishment of neuropathological disease hallmarks, thus making it unlikely that the absence of full recovery was a consequence of delayed therapeutic interventions. Overall, the evidence from postnatal m*Htt* targeting studies further suggests that additional pathogenic mechanisms are operating in response to the presence of m*Htt* during adult life.

Different studies have shown the involvement of multiple striatal cell types (MSNs, GINs, oligodendrocytes, and astrocytes) in addition to other cardinal brain regions and cell types in HD (34–37). All of these cellular subtypes are elaborated in a regional- and temporal-specific manner during neural development. Striatal cell types are, for example, derived from distinct regional ventral telencephalic progenitor pools, with MSNs derived from the lateral ganglionic eminence and GINs derived preferentially from the medial ganglionic eminence. These and other cellular components of the evolving striatum define an integrated functional microenvironment. In the context of m*Htt*, impairments of these and other striatal cellular subtypes likely contribute to progressive dysfunction of multiple regional progenitor domains, including the striatum. The presence of these developmental alterations would suggest a mechanism for generating both temporal and spatial cellular vulnerabilities that are known to occur in HD.

We have observed a change in the proportion of cells undergoing corticostriatal LTD and LTP after delivering HFS to the motor cortex in both Q97 and Q97^{CRE} mice in comparison to CTL mice (Fig. 5). Although these alterations can be explained by loss in corticostriatal functional connectivity, other mechanisms must also contribute to these alterations. One possibility for the decreased proportion of cells undergoing LTD reflects impairments in different mechanisms of striatal LTD. As a proof of principle, we have previously demonstrated that using an antagonist (AM251) of cannabinoid receptor 1 (CBR1), we reduced the proportion of cells undergoing LTD in freely moving mice (24). These findings suggest that alterations in CBR1 or other components of the signaling pathways of striatal LTD could contribute to the corticostriatal plasticity defects in HD. Accordingly, patients with HD and mouse models display alterations in molecular components of striatal LTD, including cannabinoid receptors (38–40) and the mGluR5 signaling pathway (41–43). Previous studies have shown that using an agonist for CBR1 (WIN 55,212-2) (44) or mGluR5 (42, 45) modulators in HD mouse models ameliorates several alterations associated with corticostriatal dysfunction. Alterations in excitatory-inhibitory (E-I) balance can also deregulate corticostriatal plasticity (46). Changes in inhibitory (47, 48) and excitatory (14, 17) inputs to different striatal neurons (MSN-D1 and MSN-D2, fast-spiking interneurons, and persistent low-threshold interneurons) have been observed in BACHD (at both 2 and 12 mo of age) (47) and other mouse models of HD, thereby suggesting another mechanism to explain the alterations in corticostriatal plasticity. These defects in E-I balance may be established during development, given the fact that associated synaptic alterations are present very early in HD mouse models. These overall observations suggest that the alterations in corticostriatal plasticity may be mediated by multiple mechanisms occurring in parallel, including those mechanisms exhibiting a developmental origin.

Although the use of mice carrying a mixed C57BL-6J/FVB-NJ background might potentially act as a confounding factor in our analyses, this possibility seems unlikely because (*i*) the HD-like phenotype exhibited by our mixed C57BL-6J/FVB-NJ BACHD (Q97) strain was similar to the HD-like phenotype previously described in other studies using the FVB-NJ BACHD strain, thus indicating that the mixed background did not alter the pathogenic effects of mHtt in our mouse model (9); (*ii*) Q97 and Q97^{CRE} HD-like phenotypes (e.g., neuronal vulnerability to excitotoxicity and neuronal degeneration, electrophysiological abnormalities) were consistently observed to be in the same direction throughout our studies, despite the fact that these phenotypes involved cohorts of mice obtained from different litter pools; (*iii*) our findings of neuronal degeneration and impairments of motor coordination were further confirmed in a separate cohort of experimental mice in which the FVB-NJ background was outbred following 10 consecutive matings with WT C57BL mice (Fig. S4); and (*iv*) our corticostriatal communications and plasticity experiments were performed using our purebred C57BL mouse models (Fig. 5), and both Q97 and Q97^{CRE} mice display similar alterations compared with CTL mice. These convergent observations suggest that mHtt is sufficient to produce robust pathological impairments, NMDA-mediated excitotoxicity, behavioral abnormalities, and electrophysiological alterations under these breeding paradigms.

These studies illuminate a developmental window associated with HD pathogenesis that has major implications for our understanding of the mechanisms governing the process of neurodegeneration. These observations have the potential to identify new classes of biomarkers and innovative therapeutic targets to delay, reverse, or prevent the onset and progression of HD, with potential relevance to other neurodegenerative diseases. In fact, the stages of premanifest HD likely represent the time interval during which therapeutic strategies "may provide the most positive possible outcome for patients and their families affected by this devastating disease" (5). Our findings also suggest that disease-specific profiles of propagation throughout the neuraxis are likely due to regional cellular vulnerabilities programmed during neural development rather than exclusively or preferentially due

to mechanisms of prion-like propagation of pathogenic forms of neurodegenerative disease proteins (49).

Materials and Methods

Mouse Models. All studies were conducted with the approval of the Albert Einstein Animal Institute and were in compliance with all ethical guidelines and regulations (Institutional Review Board #00023382). CTL mice (Fig. 3) encompassed a combination of WT and CAG-CRE^{ER} mice; we confirmed that there were no behavioral differences among them (Fig. S5). Detailed breeding paradigms are described in *SI Materials and Methods*.

Experimental Procedures. Detailed descriptions of all of our experimental procedures, including mouse models, behavioral tests, in vivo electrophysiology, tissue processing and staining, immunoblots, cell quantification and striatal volumetric analyses, QA stress paradigms, QRT-PCR, and statistical analyses, can be found in *SI Materials and Methods*.

ACKNOWLEDGMENTS. This work was supported by US NIH Grant NS073758 (to A.E.M.); Grant NS079750 (to K.K.); and Grants NS071571 (EUREKA), NS096144, and HD071593, as well as by grants from the F. M. Kirby, Alpern Family, Harold and Isabel Feld, and Roslyn and Leslie Goldstein Foundations (to M.F.M.).

1. Molero AE, et al. (2009) Impairment of developmental stem cell-mediated striatal neurogenesis and pluripotency genes in a knock-in model of Huntington's disease. *Proc Natl Acad Sci USA* 106(51):21900–21905.
2. Molina-Calavita M, et al. (2014) Mutant huntingtin affects cortical progenitor cell division and development of the mouse neocortex. *J Neurosci* 34(30):10034–10040.
3. Cummings DM, et al. (2006) Aberrant cortical synaptic plasticity and dopaminergic dysfunction in a mouse model of Huntington's disease. *Hum Mol Genet* 15(19): 2856–2868.
4. Nopoulos PC, et al.; PREDICT-HD Investigators and Coordinators of the Huntington Study Group (2011) Smaller intracranial volume in prodromal Huntington's disease: Evidence for abnormal neurodevelopment. *Brain* 134(Pt 1):137–142.
5. Paulsen JS, et al.; PREDICT-HD Investigators and Coordinators of the Huntington Study Group (2014) Clinical and Biomarker Changes in Premanifest Huntington Disease Show Trial Feasibility: A Decade of the PREDICT-HD Study. *Front Aging Neurosci* 6:78.
6. Rossi S, et al. (2006) Deficits of glutamate transmission in the striatum of toxic and genetic models of Huntington's disease. *Neurosci Lett* 410(1):6–10.
7. Tabrizi SJ, et al.; TRACK-HD Investigators (2013) Predictors of phenotypic progression and disease onset in premanifest and early-stage Huntington's disease in the TRACK-HD study: Analysis of 36-month observational data. *Lancet Neurol* 12(7):637–649.
8. Ross CA, Tabrizi SJ (2011) Huntington's disease: From molecular pathogenesis to clinical treatment. *Lancet Neurol* 10(1):83–98.
9. Gray M, et al. (2008) Full-length human mutant huntingtin with a stable polyglutamine repeat can elicit progressive and selective neuropathogenesis in BACHD mice. *J Neurosci* 28(24):6182–6195.
10. Hayashi S, McMahon AP (2002) Efficient recombination in diverse tissues by a tamoxifen-inducible form of Cre: A tool for temporally regulated gene activation/inactivation in the mouse. *Dev Biol* 244(2):305–318.
11. Graham RK, et al. (2009) Differential susceptibility to excitotoxic stress in YAC128 mouse models of Huntington disease between initiation and progression of disease. *J Neurosci* 29(7):2193–2204.
12. Zeron MM, et al. (2002) Increased sensitivity to N-methyl-D-aspartate receptor-mediated excitotoxicity in a mouse model of Huntington's disease. *Neuron* 33(6): 849–860.
13. Kudwa AE, et al. (2013) Increased Body Weight of the BAC HD Transgenic Mouse Model of Huntington's Disease Accounts for Some but Not All of the Observed HD-like Motor Deficits. *PLoS Curr* 5. Available at www.ncbi.nlm.nih.gov/pmc/articles/PMC3770835/.
14. André VM, et al. (2011) Differential electrophysiological changes in striatal output neurons in Huntington's disease. *J Neurosci* 31(4):1170–1182.
15. Cayzac S, Delcasso S, Paz V, Jeantet Y, Cho YH (2011) Changes in striatal procedural memory coding correlate with learning deficits in a mouse model of Huntington disease. *Proc Natl Acad Sci USA* 108(22):9280–9285.
16. Cepeda C, et al. (2003) Transient and progressive electrophysiological alterations in the corticostriatal pathway in a mouse model of Huntington's disease. *J Neurosci* 23(3):961–969.
17. Joshi PR, et al. (2009) Age-dependent alterations of corticostriatal activity in the YAC128 mouse model of Huntington disease. *J Neurosci* 29(8):2414–2427.
18. Berke JD, Okatan M, Skurski J, Eichenbaum HB (2004) Oscillatory entrainment of striatal neurons in freely moving rats. *Neuron* 43(6):883–896.
19. Deng YP, Wong T, Bricker-Anthony C, Deng B, Reiner A (2013) Loss of corticostriatal and thalamostriatal synaptic terminals precedes striatal projection neuron pathology in heterozygous Q140 Huntington's disease mice. *Neurobiol Dis* 60:89–107.
20. McKinstry SU, et al. (2014) Huntingtin is required for normal excitatory synapse development in cortical and striatal circuits. *J Neurosci* 34(28):9455–9472.
21. Plotkin JL, et al. (2014) Impaired TrkB receptor signaling underlies corticostriatal dysfunction in Huntington's disease. *Neuron* 83(1):178–188.
22. Picconi B, et al. (2003) Loss of bidirectional striatal synaptic plasticity in L-DOPA-induced dyskinesia. *Nat Neurosci* 6(5):501–506.
23. Thiele SL, et al. (2014) Selective loss of bi-directional synaptic plasticity in the direct and indirect striatal output pathways accompanies generation of parkinsonism and l-DOPA induced dyskinesia in mouse models. *Neurobiol Dis* 71:334–344.
24. Chen CH, Fremont R, Arteaga-Bracho EE, Khodakhah K (2014) Short latency cerebellar modulation of the basal ganglia. *Nat Neurosci* 17(12):1767–1775.
25. Lorincz MT, Zawistowski VA (2009) Expanded CAG repeats in the murine Huntington's disease gene increases neuronal differentiation of embryonic and neural stem cells. *Mol Cell Neurosci* 40(1):1–13.
26. Nguyen GD, Gokhan S, Molero AE, Mehler MF (2013) Selective roles of normal and mutant huntingtin in neural induction and early neurogenesis. *PLoS One* 8(5):e64368.
27. Mehler MF, Gokhan S (2001) Developmental mechanisms in the pathogenesis of neurodegenerative diseases. *Prog Neurobiol* 63(3):337–363.
28. Kordasiewicz HB, et al. (2012) Sustained therapeutic reversal of Huntington's disease by transient repression of huntingtin synthesis. *Neuron* 74(6):1031–1044.
29. Rodriguez-Lebron E, Denovan-Wright EM, Nash K, Lewin AS, Mandel RJ (2005) Intrastriatal rAAV-mediated delivery of anti-huntingtin shRNAs induces partial reversal of disease progression in R6/1 Huntington's disease transgenic mice. *Mol Ther* 12(4): 618–633.
30. Wang H, et al. (2006) Suppression of polyglutamine-induced toxicity in cell and animal models of Huntington's disease by ubiquilin. *Hum Mol Genet* 15(6):1025–1041.
31. Boudreau RL, et al. (2009) Nonallele-specific silencing of mutant and wild-type huntingtin demonstrates therapeutic efficacy in Huntington's disease mice. *Mol Ther* 17(6):1053–1063.
32. Yamamoto A, Lucas JJ, Hen R (2000) Reversal of neuropathology and motor dysfunction in a conditional model of Huntington's disease. *Cell* 101(1):57–66.
33. Harper B (2005) Huntington disease. *J R Soc Med* 98(12):550.
34. Kim EH, et al. (2014) Cortical interneuron loss and symptom heterogeneity in Huntington disease. *Ann Neurol* 75(5):717–727.
35. Myers RH, et al. (1991) Decreased neuronal and increased oligodendroglial densities in Huntington's disease caudate nucleus. *J Neuropathol Exp Neurol* 50(6):729–742.
36. Reiner A, et al. (1988) Differential loss of striatal projection neurons in Huntington disease. *Proc Natl Acad Sci USA* 85(15):5733–5737.
37. Tong X, et al. (2014) Astrocyte Kir4.1 ion channel deficits contribute to neuronal dysfunction in Huntington's disease model mice. *Nat Neurosci* 17(5):694–703.
38. Glass M, Dragunow M, Faull RL (2000) The pattern of neurodegeneration in Huntington's disease: A comparative study of cannabinoid, dopamine, adenosine and GABA(A) receptor alterations in the human basal ganglia in Huntington's disease. *Neuroscience* 97(3):505–519.
39. Lastres-Becker I, et al. (2002) Loss of mRNA levels, binding and activation of GTP-binding proteins for cannabinoid CB1 receptors in the basal ganglia of a transgenic model of Huntington's disease. *Brain Res* 929(2):236–242.
40. Pouladi MA, et al. (2012) Marked differences in neurochemistry and aggregates despite similar behavioural and neuropathological features of Huntington disease in the full-length BACHD and YAC128 mice. *Hum Mol Genet* 21(10):2219–2232.
41. Ribeiro FM, Paquet M, Cregan SP, Ferguson SS (2010) Group I metabotropic glutamate receptor signalling and its implication in neurological disease. *CNS Neurol Disord Drug Targets* 9(5):574–595.
42. Ribeiro FM, et al. (2010) Metabotropic glutamate receptor-mediated cell signaling pathways are altered in a mouse model of Huntington's disease. *J Neurosci* 30(1): 316–324.
43. Ribeiro FM, Pires RG, Ferguson SS (2011) Huntington's disease and Group I metabotropic glutamate receptors. *Mol Neurobiol* 43(1):1–11.
44. Chiodi V, et al. (2012) Unbalance of CB1 receptors expressed in GABAergic and glutamatergic neurons in a transgenic mouse model of Huntington's disease. *Neurobiol Dis* 45(3):983–991.
45. Doria JG, et al. (2013) Metabotropic glutamate receptor 5 positive allosteric modulators are neuroprotective in a mouse model of Huntington's disease. *Br J Pharmacol* 169(4):909–921.
46. Paille V, et al. (2013) GABAergic circuits control spike-timing-dependent plasticity. *J Neurosci* 33(22):9353–9363.
47. Cepeda C, et al. (2013) Multiple sources of striatal inhibition are differentially affected in Huntington's disease mouse models. *J Neurosci* 33(17):7393–7406.
48. Dvorzhak A, Semtner M, Faber DS, Grantyn R (2013) Tonic mGluR5/CB1-dependent suppression of inhibition as a pathophysiological hallmark in the striatum of mice carrying a mutant form of huntingtin. *J Physiol* 591(4):1145–1166.
49. Frost B, Diamond MI (2010) Prion-like mechanisms in neurodegenerative diseases. *Nat Rev Neurosci* 11(3):155–159.
50. Gulinello M, et al. (2010) Acquired infection with Toxoplasma gondii in adult mice results in sensorimotor deficits but normal cognitive behavior despite widespread brain pathology. *Microbes Infect* 12(7):528–537.
51. Stanley JL, et al. (2005) The mouse beam walking assay offers improved sensitivity over the mouse rotarod in determining motor coordination deficits induced by benzodiazepines. *J Psychopharmacol* 19(3):221–227.
52. du Hoffmann J, Kim JJ, Nicola SM (2011) An inexpensive drivable cannulated microelectrode array for simultaneous unit recording and drug infusion in the same brain nucleus of behaving rats. *J Neurophysiol* 106(2):1054–1064.
53. Takekawa T, Isomura Y, Fukai T (2010) Accurate spike sorting for multi-unit recordings. *Eur J Neurosci* 31(2):263–272.
54. Gundersen HJ, Jensen EB (1987) The efficiency of systematic sampling in stereology and its prediction. *J Microsc* 147(Pt 3):229–263.
55. Schneider CA, Rasband WS, Eliceiri KW (2012) NIH Image to ImageJ: 25 years of image analysis. *Nat Methods* 9(7):671–675.